Bi-alkali antimonide photocathode growth: An X-ray diffraction study

Susanne Schubert,[1,2] Jared Wong,[1] Jun Feng,[1] Siddharth Karkare,[1,a)] Howard Padmore,[1]
Miguel Ruiz-Osés,[2,b)] John Smedley,[2] Erik Muller,[2] Zihao Ding,[2] Mengjia Gaowei,[2]
Klaus Attenkofer,[2] Xue Liang,[2] Junqi Xie,[3] and Julius Kühn[4]
[1]*Lawrence Berkeley National Laboratory, 1 Cyclotron Road, Berkeley, California 94720, USA*
[2]*Brookhaven National Laboratory, Upton, New York 11973, USA*
[3]*Argonne National Laboratory, 9700 South Cass Avenue B109, Lemont, Illinois 60439, USA*
[4]*Helmholtz-Zentrum Berlin, Albert-Einstein Strasse 15, Berlin 12489, Germany*

Bi-alkali antimonide photocathodes are one of the best known sources of electrons for high current and/or high bunch charge applications like Energy Recovery Linacs or Free Electron Lasers. Despite their high quantum efficiency in visible light and low intrinsic emittance, the surface roughness of these photocathodes prohibits their use as low emittance cathodes in high accelerating gradient superconducting and normal conducting radio frequency photoguns and limits the minimum possible intrinsic emittance near the threshold. Also, the growth process for these materials is largely based on recipes obtained by trial and error and is very unreliable. In this paper, using X-ray diffraction, we investigate the different structural and chemical changes that take place during the growth process of the bi-alkali antimonide material K_2CsSb. Our measurements give us a deeper understanding of the growth process of alkali-antimonide photocathodes allowing us to optimize it with the goal of minimizing the surface roughness to preserve the intrinsic emittance at high electric fields and increasing its reproducibility. *Published by AIP Publishing.*
[http://dx.doi.org/10.1063/1.4959218]

I. INTRODUCTION

A wide range of electron accelerator-based projects need photoinjectors capable of high current and low emittance operation. The high repetition rate of Energy Recovery Linacs (ERLs) and a new generation of Free Electron Lasers (FELs) requires that the photocathode used in the photoinjector operate with a high quantum efficiency (QE) and lowest possible intrinsic emittance. The high QE is required so that the requirements on the laser used for photoemission can be reasonable[1] and the lowest possible intrinsic emittance is required to minimize the emittance of the electron beam obtained from a photoinjector,[2] thus maximizing the electron beam brightness. In order to allow simpler longitudinal and transverse beam shaping, high sensitivity in the visible part of the spectrum is desired. Additionally, in order to deliver high beam currents for extended periods of time the cathode needs to be robust to vacuum conditions.[3]

The only cathode materials that satisfy these constraints are the alkali antimonides, for example, K_2CsSb. These materials offer a QE of up to 10% in the green (532 nm), with low intrinsic emittance ($\sim$0.36 μm per mm rms laser spot size).[4,5] Due to its robustness to vacuum conditions compared to other high QE cathodes such as negative electron affinity GaAs, K_2CsSb is the only known cathode material suitable for high current applications and holds the world record for the highest current delivered from any photoinjector.[3] Alkali-antimonides have also been used to demonstrate bunch charges as high as 2 nC from high gradient superconducting radio frequency

guns;[6] however, no measurement of intrinsic emittance of the cathode has been made at high gradients.

K_2CsSb photocathodes are typically grown as thin films over conducting substrates by thermal evaporation of $\sim$10–30 nm of Sb followed by sequential thermal evaporation of K and Cs, respectively.[7,8] The films created by this process are not ordered and typically have a root mean square (rms) surface roughness of 25 nm with a period of roughly 100 nm.[9] Low emittance operation of cathodes grown using this technique has been successfully demonstrated in DC photoguns where the electric field at the cathode surface is limited to a few MV/m. However, high bunch charge applications require electric fields at the cathode to be larger than 15–20 MV/m. It is possible to obtain such electric fields in superconducting or normal conducting radio frequency guns.[6] At such electric fields, it is expected that the intrinsic emittance due to a rough photocathode surface will be larger than 2 μm per mm rms laser spot size[10] prohibiting their use for such applications. Further, such a surface roughness also limits the smallest possible intrinsic emittance obtained from alkali-antimonide photocathodes at the photoemission threshold even at low electric fields. In smooth metallic photocathodes, the smallest intrinsic emittance is obtained at the photoemission threshold and is limited by the temperature of the substrate.[11] However, the surface roughness is thought to limit the intrinsic emittance of alkali-antimonide cathodes to a 50% larger value than the thermal limit.[12] This limit becomes even more severe for applications where lower emittance is required, such as for ultrafast electron diffraction or FELs, where transverse temperature is reduced by reduction of substrate temperature and by use of directional photoemission.[13] In this regime, with reasonable

accelerating fields of, for example, 20 MV/m, sub nm surface roughness is required. Understanding the growth mode in detail, with the aim of being able to control roughening is of the utmost importance in the development of low transverse momentum photocathodes.

Apart from the surface roughness, another drawback of the growth process of alkali-antimonide photocathodes is its unreliability and is extreme sensitivity to the temperature, pressure, and deposition rates. This makes it nearly impossible to reproduce the exact growth procedure and adjustments in substrate temperature and deposition rates need to be made continuously, every time a cathode is grown.[14] The recipes followed for growing alkali antimonide materials are largely obtained by a trial and error process while trying to maximize the quantum efficiency without any understanding of the chemical and structural changes that take place on the surface during the growth. Such changes can be very sensitive to the growth conditions and are the cause of the surface roughness.[7] It is essential to understand these changes in order to develop reliable growth procedures that minimize the surface roughness of alkali antimonide cathodes.

In this paper, we have used *in-situ* X-ray diffraction (XRD) to study the structure of the thin film during the various stages of the deposition of K_2CsSb photocathodes at different substrate temperatures. We detail the various structural and chemical transformations that take place during the growth of the thin film and study the effect of the substrate temperature on these transformations. The knowledge of these changes will allow us to optimize the growth recipes in order to minimize the surface roughness and increase the reproducibility.

II. EXPERIMENTAL DETAILS

In-situ X-ray diffraction growth studies on K_2CsSb were performed at the National Synchrotron Light Source (NSLS) beamline X21 and the Cornell High Energy Synchrotron Source (CHESS) beamline G3. The X-ray measurements were performed using photon energies between 9.8 and 11.3 keV. X-ray scattering was used to monitor the samples *in-situ* throughout the growth. Samples were grown on p-doped Si(100) substrates through thermal evaporation in ultrahigh vacuum (UHV) with a base pressure of 1×10^{-10} Torr. The $1 \text{ cm} \times 2 \text{ cm}$ Si substrates were first rinsed in Acetone for 30 min, then rinsed in Isopropyl Alcohol (IPA) for 30 min. The substrates were dried with dry nitrogen and then etched in dilute hydrofluoric acid (HF) for 5 min in order to remove the native oxide and to hydrogen passivate the surface. After the HF treatment, the Si substrates were rinsed and stored in deionized (DI) water to minimize re-oxidation of the Si surface. The substrates were loaded into the growth chamber and annealed at 500 °C for 3 h, then cooled to the desired substrate temperature (T_S) at which the material was deposited.

Following the standard growth technique, the photocathode material was grown in a sequential manner. First, 15 nm of Sb was thermally evaporated from PtSb beads with a rate of 0.2 Å/s. This type of source has been shown to produce smoother films than evaporation from elemental Sb[15] due to the formation of monomers in the gas phase, rather than the small clusters formed in evaporation from bulk material.[16] Such films usually show an out-of-plane roughness in the sub-nanometer range, e.g., around 3 Å for a 15 nm film.[17] Following deposition of Sb, K is evaporated until a maximum is observed in the photoyield. Typically, this maximum gives a QE of 0.05%–0.1% and corresponds to 70–90 nm of K layer thickness. Following this, Cs is evaporated until a photoyield maximum is reached. This results in 3%–10% QE with $\sim$90–120 nm of Cs deposited. The alkali metals were evaporated from commercial alkali-Bismuth dewetting sources (Alvatech). The thickness of each material was measured with a quartz crystal thin film monitor (QCM). The values of thickness measured are subject to uncertainty due to several factors. The sticking coefficient of the materials on the sample at elevated temperature will be different compared to the sticking coefficient on the room temperature monitor. In addition, the sticking coefficient on the monitor will depend on its previous deposition history. Nevertheless, the monitor gives a rough guide to the amount of material deposited, and also is useful for setting up similar conditions between different evaporations.

The photocurrent was measured using a Keithley 6517B electrometer and a 5.5 mW 532 nm laser as the light source. An optical filter was used to reduce the intensity of the laser light to avoid space-charge effects and the intensity was measured with a thermopile detector. The temperature of the sample could be varied using a resistive heater, and the temperature was monitored directly with a thermocouple. X-ray diffraction (XRD) measurements were performed in a $\theta/2\theta$ geometry from a 2θ of 10° to 35°, using an incident beam size of 0.5×1 mm. A Pilatus 100 K X-ray pixel detector which provides single photon detection sensitivity was used. Details of the experimental setup can be found elsewhere.[7]

III. RESULTS AND DISCUSSION

A. Growth dynamics

Below we present the XRD measurements obtained from two samples during growth. The substrate of the first sample was kept at room temperature during the growth, whereas the substrate of the second sample was kept at 100 °C. From these measurements, the dynamics of the Sb layer deposition, conversion to K_3Sb during K deposition, and subsequent conversion to K_2CsSb during Cs deposition can be studied.

1. Substrate at room temperature

Figure 1(a) shows XRD measurements of the Sb layer for every 2 nm interval steps in the growth of the sample at room temperature. Beyond 6 nm of Sb growth, a single peak at d = 3.757 Å corresponding to the (003) orientation of Sb is observed. This shows that the antimony grows in a crystalline form with (003) as the preferred orientation at room temperature.

K was deposited on this Sb layer at room temperature. XRD measurements were taken in 10 nm interval steps during the K layer deposition. The results obtained from this measurement are presented in Figure 1(b). After the K layer
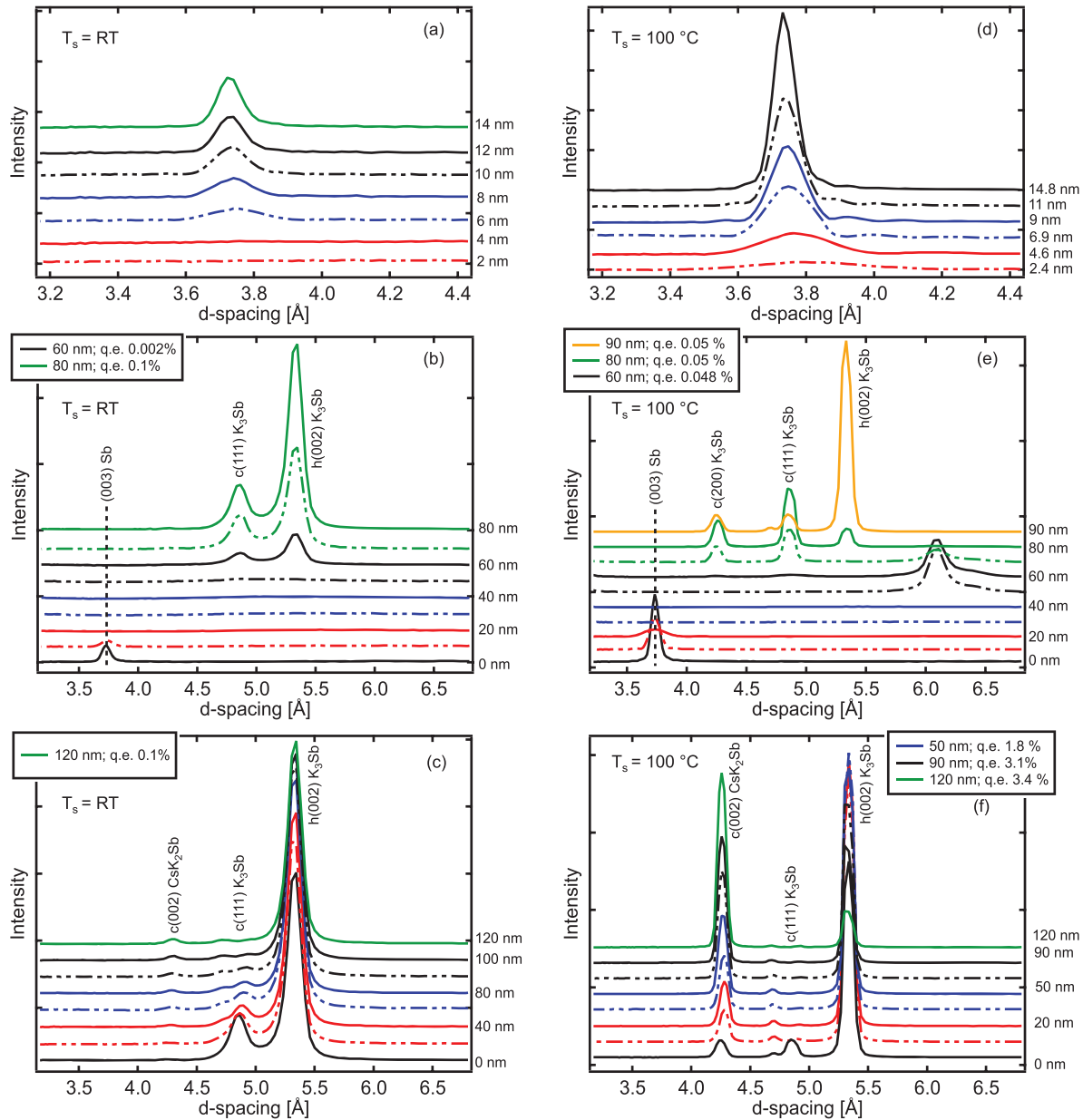
FIG. 1. XRD spectra taken during the growth of K_2CsSb. Indicated are relevant diffraction peaks. Sb grown at $T_S = RT$ (a) and $T_S = 100\,°C$ (d) in 2 nm steps. K deposition on Sb films shown in (a) and (d) at $T_S = RT$ (b) and $T_S = 100\,°C$ (e) in 10 nm deposition steps. Cs deposition on preceding K-Sb phase from (b) and (e) in 10–20 nm steps for $T_S = RT$ (c) and $T_S = 100\,°C$ (f) respectively.

thickness reaches 20 nm, the Sb(003) peak disappears indicating the formation of a K-Sb amorphous mixture. As K deposition continues, the mixture reaches a threshold at 60 nm of K deposition and crystallizes to form only the hexagonal (h(002) peak) and the cubic (c(111) peak) phases of K_3Sb. The K deposition was continued till 80 nm thickness of the K layer was achieved. At this stage, a QE of 0.1% was obtained.

Figure 1(c) shows the XRD measurements for 20 nm interval steps in the Cs layer deposition on this K_3Sb layer at room temperature. Cs readily reacts with the cubic phase of K_3Sb to form the cubic phase of K_2CsSb even at room temperature as indicated by the disappearance of the c(111) peak of K_3Sb and appearance of the c(002) peak of K_2CsSb with increasing Cs layer thickness. The h(002) peak of K_3Sb

decreases by a very small amount indicating that most of the K_3Sb in the hexagonal phase remains unreacted up to this point in deposition at room temperature. Even after 120 nm of Cs deposition the QE does not increase much beyond 0.1%.

2. Substrate at 100 °C

Figure 1(d) shows XRD measurements of the Sb layer for 2 nm interval steps in the growth when the substrate was at 100 °C. As in the room temperature case, a single peak at $d = 3.757\,\text{Å}$ corresponding to the (003) orientation of Sb is observed. However, the elevated substrate temperature in this case causes the Sb to crystallize much faster and the peak can be seen beyond only 2 nm of Sb deposition. The
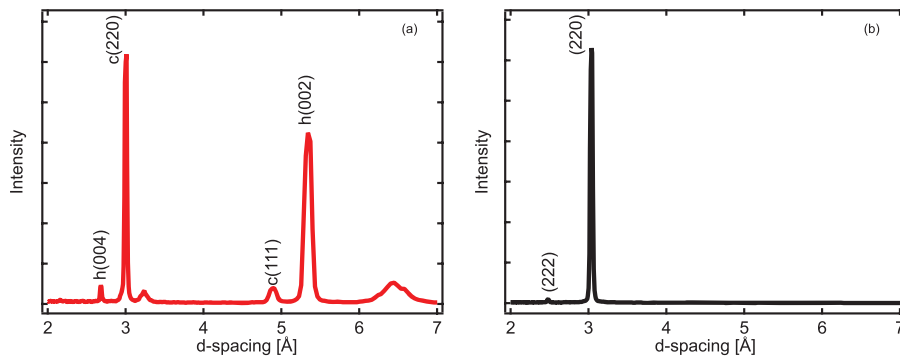
FIG. 2. XRD of K-Sb phase (a) and K_2CsSb (b) grown at $T_S = 100\,°C$ without interruptions. In (a) diffraction peaks corresponding to cubic and hexagonal K_3Sb are indicated, as well present diffraction peaks of other K-Sb crystalline phases, no peak assignment. (b) The diffraction pattern of the K_2CsSb phase after reaction of Cs with (a).

crystal sizes as calculated from Scherrer's equation[18] are about 10% larger as compared to room temperature deposition. The intensity of this peak is much higher than that obtained at room temperature deposition (Figure 1(a)) due to a higher degree of crystallinity.

Figure 1(e) shows XRD measurements in 10 nm interval steps in the K layer deposition on this Sb layer at $100\,°C$. Compared to the room temperature case, the reaction of Sb and K at $100\,°C$ is much more complex. As in the room temperature case, during the deposition of K, the Sb structure is dissolved forming a K-Sb amorphous mixture beyond 20 nm K layer thickness as evidenced by the disappearance of the Sb(003) peak. However in this case several intermediate phases of K_xSb_y are formed at ~50–60 nm of K layer thickness. These phases disappear at ~70 nm of K layer thickness to form the cubic phase of K_3Sb, with the diffraction peaks of the (200) and (111) plane detectable. By 80 nm of K layer thickness, the hexagonal phase begins to form, h(002) peak, and by 90 nm it becomes the dominant phase. The QE remains nearly constant at 0.05% between 60–90 nm of K layer thickness. With a substrate temperature of $100\,°C$, the additional thermal energy aids in the reaction between Sb and K; however, it also increases the mobility of the K atoms and impedes the sticking of K to the surface causing the complex intermediate phases that quickly transform to the cubic and finally to the hexagonal K_3Sb phases. It is interesting to note the various phase changes that occur in the K-Sb layer caused by only small additions of K and that the QE remains nearly constant during this phase transition.

Figure 1(f) shows XRD measurements in 10–20 nm interval steps in the Cs layer deposition on this K_3Sb layer at $100\,°C$. Cs reacts very quickly with the cubic phase of K_3Sb to form K_2CsSb at only 10 nm of Cs layer thickness. The hexagonal K_3Sb starts to convert much later, after approximately 70 nm of Cs is deposited. After 120 nm of Cs deposition, most of the hexagonal K_3Sb structure is converted and the sample is mainly K_2CsSb. The QE at this stage was measured to be 3.4%. At this point, the film is comprised mainly of cubic K_2CsSb with a small portion of unreacted hexagonal K_3Sb.

B. Conversion to K_2CsSb

The results of Sec. III A clearly show that compared to the cubic phases of K_3Sb, the hexagonal phase is more stable and more difficult to convert to K_2CsSb. In fact, at room

temperature no conversion of the hexagonal K_3Sb phase was detectable. The difference in transformation of the two K_3Sb phases can be explained by looking into their crystal structure. For the transformation of cubic K_3Sb into cubic K_2CsSb, cesium has to replace one K-atom, and this is more difficult for the closely packed hexagonal lattice. Also, the cubic phase is usually already alkali deficient, facilitating the incorporation of Cs atoms.[19] Transforming the hexagonal structure involves not only the exchange of atoms but also the break-down of a very stable crystal structure and the rebuilding of a new structure. This would make the hexagonal structure highly unfavorable for converting K_3Sb to K_2CsSb.

In order to demonstrate full conversion to K_2CsSb, we grew another sample at an elevated substrate temperature of $100\,°C$. The growth consisted of 15 nm Sb and only 70 nm K. The XRD results from this K-Sb layer are shown in Figure 2(a). It can be seen that most of the K-Sb is in a mixed phase comprising of the cubic, hexagonal, and the intermediate K_xSb_y structures. Proportionately smaller amount of Cs (i.e., 90 nm of Cs) was deposited on this K-Sb film. The XRD measurements of the resulting K_2CsSb film are shown in Figure 2(b). It can be seen that full conversion to K_2CsSb has been achieved with only 90 nm of Cs. This sample resulted in a QE of 6.7%. From this measurement, we can conclude that easiest conversion of K_3Sb to K_2CsSb occurs when the K_3Sb is not in its stable hexagonal phase but is in the less stable cubic phase.

IV. SUMMARY AND CONCLUSION

In summary, we showed that elevated substrate temperatures simply lead to more crystalline structure in Sb thin films. However, we see that the temperature effects are more complex for the deposition and reaction with K. The reaction of K with Sb at elevated substrate temperatures goes through several phase transformations which are not detected during the reaction at room temperature. These phase transformations are very sensitive to the thickness of the K layer deposited and the substrate temperature. With $T_S = 100\,°C$, the additional thermal energy aids in the reaction between Sb and K; however, it also increases the mobility of the K atoms and impedes the sticking properties of K. The elevated temperature causes faster and different reactions which result in a mixed KSb phase that quickly transforms to cubic K_3Sb and finally to hexagonal K_3Sb. Also, the QE may remain

nearly constant during these phase transitions. The RT growth shows that without the extra thermal energy, diffusion and hence the reaction of K and Sb are impaired. Therefore, only after sufficient K is present, the Sb film converts to the most stable crystalline K-Sb phase, namely, K_3Sb.

The conversion of K_3Sb to K_2CsSb through the deposition of Cs seems to take similar paths regardless of sample temperature. The cubic structure of K_3Sb converts first followed by the hexagonal phase much later. Substrate temperature does play a role in the conversion of the hexagonal phase and it is apparent that additional thermal energy is needed for conversion to K_2CsSb. Finally, we see that a sample with a mixture of many K_xSb_y intermediate phases gets easily and fully converted to K_2CsSb yielding the best quality K_2CsSb and showing that the conversion to K_2CsSb is dramatically affected by the phase of the K_3Sb layer.

In conclusion, the sensitivity of the phase change in K-Sb to the thickness of K deposited along with the preferential ease of conversion of the cubic K_3Sb phase into K_2CsSb are responsible for the unreliable growth process based only on the QE monitoring. Further, the making and breaking of the crystal structure during conversion from Sb to K-Sb to K_2CsSb is thought to be the cause of the surface roughness.[7]

Thus, we detail the various structural and chemical changes that take place during the sequential growth of K_2CsSb photocathodes. Understanding these changes is the first step in developing a reliable growth procedure for alkali antimonide photocathode materials that have smooth surfaces. Developing such procedures are crucial to the successful development of several large accelerators based on ERL and FEL technologies.

ACKNOWLEDGMENTS

[1]D. Dowell, I. Bazarov, B. Dunham, K. Harkay, C. Hernandez-Garcia, R. Legg, H. Padmore, T. Rao, J. Smedley, and W. Wan, Nucl. Instrum. Methods Phys. Res., Sect. A **622**, 685 (2010).

[2]C. Gulliford, A. Bartnik, I. Bazarov, L. Cultrera, J. Dobbins, B. Dunham, F. Gonzalez, S. Karkare, H. Lee, H. Li, Y. Li, X. Liu, J. Maxson, C. Nguyen, K. Smolenski, and Z. Zhao, Phys. Rev. Spec. Top.–Accel. Beams **16**, 073401 (2013).

[3]B. Dunham, A. Bartnik, I. Bazarov, L. Cultrera, J. Dobbins, G. Hoffstaetter, B. Johnson, R. Kaplan, V. Kostroun, S. Karkare, Y. Li, M. Liepe, X. Lui, F. Loehl, J. Maxson, P. Quigley, D. Reilly, D. Rice, D. Sobol, E. Smith, K. Smolenski, M. Tigner, V. Veshcherevich, and Z. Zhao, Appl. Phys. Lett. **102**, 034105 (2013).

[4]T. Vecchione, I. Ben-Zvi, D. H. Dowell, J. Feng, T. Rao, J. Smedley, W. Wan, and H. A. Padmore, Appl. Phys. Lett. **99**, 034103 (2011).

[5]I. Bazarov, L. Cultrera, A. Bartnik, B. Dunham, S. Karkare, Y. Li, X. Lui, J. Maxson, and W. Roussel, Appl. Phys. Lett. **98**, 224101 (2011).

[6]I. Pinayev, Z. Altinbas, S. Belomestnykh, I. Ben-Zvi, K. Brown, J. Brutus, A. Curcio, A. DiLieto, C. Folz, D. Gassner *et al.*, in Proceedings of the IPAC (2016), Paper No. WEOAB02.

[7]M. Ruiz-Osés, S. Schubert, K. Attenkofer, I. Ben-Zvi, X. Liang, E. Muller, H. Padmore, T. Rao, T. Vecchione, J. Wong, J. Xie, and J. Smedley, APL Mater. **2**, 121101 (2014).

[8]L. Cultrera, I. Bazarov, J. V. Conway, B. Dunham, S. Karkare, Y. Li, X. Liu, J. Maxson, and K. Smolenski, in Proceedings of the IPAC (2011), Paper No. WEP244.

[9]S. Schubert, M. Ruiz-Osés, I. Ben-Zvi, T. Kamps, X. Liang, E. Muller, K. Mueller, H. Padmore, T. Rao, X. Tong, T. Vecchione, and J. Smedley, APL Mater. **1**, 032119 (2013).

[10]J. Smedley, M. Gaowei, J. Sinsheimer, K. Attenkofer, J. Walsh, S. Schubert, J. Wong, H. Padmore, J. Kuhn, E. Muller, Z. Ding, H. Frisch, H. B. Bhandari, H. Lingertat, V. Wang, O. Ovechkina, and V. V. Nagarkar, in Proceedings of the IPAC (2015), Paper No. TUPHA003.

[11]J. Feng, J. Nasiatka, W. Wan, S. Karkare, J. Smedley, and H. Padmore, Appl. Phys. Lett. **107**, 134101 (2015).

[12]L. Cultrera, S. Karkare, H. Lee, X. Liu, I. Bazarov, and B. Dunham, Phys. Rev. Spec. Top.–Accel. Beams **18**, 134101 (2015).

[13]S. Karkare and I. Bazarov, Appl. Phys. Lett. **98**, 094104 (2011).

[14]D. H. Dowell, S. Z. Bethel, and K. D. Friddell, Nucl. Instrum. Methods Phys. Res., Sect. A **356**, 167 (1995).

[15]A. H. Sommer, J. Appl. Phys. **37**, 2789 (1966).

[16]F. Baumann, J. Kessler, and W. Roessler, J. Appl. Phys. **38**, 3398 (1967).

[17]J. Smedley, K. Attenkofer, S. Schubert, T. Vecchione, J. Wong, T. Forrest, H. A. Padmore, E. Muller, X. Liang, M. Ruiz-Osés, I. Ben-Zvi, and J. Xie, in *Proceedings of the IPAC* (2013), p. 464.

[18]A. L. Patterson, Phys. Rev. **56**, 978 (1939).

[19]A. H. Sommer, J. Appl. Phys. **29**, 1568 (1958).